Spin-glass behavior in $Co_3Mn_3(O_2BO_3)_2$ ludwigite with weak disorder

M. A. V. Heringer,[1] D. L. Mariano,[1] D. C. Freitas,[1] E. Baggio-Saitovitch,[2] M. A. Continentino,[2] and D. R. Sanchez[1,*]

[1]*Instituto de Física, Universidade Federal Fluminense, Campus da Praia Vermelha, 24210-340 Niterói, Rio de Janeiro, Brazil*

[2]*Centro Brasileiro de Pesquisas Físicas, Rua Doutor Xavier Sigaud, 150-Urca 22290-180 Rio de Janeiro, Rio de Janeiro, Brazil*

(Received 7 November 2019; revised manuscript received 27 January 2020; accepted 31 March 2020; published 12 June 2020)

X-ray diffraction, magnetization, ac susceptibility, and specific heat have been measured on high-quality single crystals of $Co_3Mn_3(O_2BO_3)_2$ ludwigite. Different from previously studied ludwigites, this compound is characterized by the existence two low-dimensional subunits each containing a unique ion. The subsystem formed by ions at sites 3-1-3, known as a three-legged ladder (3LL), contains only divalent Co ions, while the 3LL formed by ions at sites 4-2-4 contains both divalent and trivalent Mn ions. Although there is only a weak disorder caused by a very small amount of Mn at sites 1, the experimental results evidence the existence of a low-temperature spin-glass phase. A dynamic scaling analysis of ac susceptibility data according to conventional critical slowing down results in a spin-glass phase-transition temperature $T_g = 31.9$ K and a dynamic exponent $z\nu = 7.05$. The temperature dependence of heat capacity has a linear contribution with the coefficient $\gamma = 21.9$ mJ/(mol K^2), which shows that this compound has the highest degree of magnetic disorder among ludwigites, corroborating the spin-glass state at low temperatures. The origin of this state is discussed, taking into account the particular structure of each subunit and the competition between the different exchange interactions involved.

DOI: 10.1103/PhysRevMaterials.4.064412

I. INTRODUCTION

In recent years, ludwigites with chemical composition $M_2M'O_2BO_3$, where M and M' are divalent and trivalent metallic ions, respectively, have been extensively studied due to their diverse electronic and magnetic properties. These include charge ordering [1], structural order [1], magnetic order [1,2], coexistence of magnetic order and paramagnetism [3], metamagnetism [2], magnetocaloric effect [4], and spin-glass-type order [5]. Behind these properties, several physical mechanisms are involved. Regarding the magnetic properties, knowledge about the role of each type of exchange interaction in the establishment of its magnetic ground states has been widely sought.

Several studies carried out in the ludwigites have shown that for a better understanding of their physical properties it is necessary, first of all, to pay attention to what happens within the low-dimensional subunits of its crystalline structure. The ludwigites consist of two types of three-legged ladders formed by ions at sites 3-1-3 and 4-2-4, as can be seen in Fig. 1. It is in the 4-2-4 ladders, where the magnetic ions are closest to each other, that the strongest magnetic interactions are expected to take place.

The archetype homometallic $Fe_3O_2BO_3$ ludwigite presents at 283 K structural and charge ordering transitions that take place in the 4-2-4 ladder [1,7]. The competition of direct-, super-, and double-exchange interactions gives rise to magnetic ordering of the Fe moments in the 4-2-4 ladders at 112 K, which coexists with the remaining magnetic ions (Fe^{2+}), at sites 1 and 3, in a paramagnetic state [1,7]. For lower temperature two successive ferromagnetic and antiferromagnetic orderings at 70 and 40 K, respectively, take place throughout the compound [1]. The Fe spins in the same crystalline site are antiferromagnetically coupled along the c axis while the coupling between sites 4 and 2 is ferromagnetic, so their magnetic structure can be seen as ferromagnetically coupled antiferromagnetic chains [3].

On the other hand, the homometallic $Co_3O_2BO_3$ ludwigite undergoes a single magnetic transition at $T_c = 43$ K throughout the compound [8]. Neutron-diffraction experiments have shown that below T_c the Co^{3+} at sites 4 are in a low-spin (LS) state [9]. In this way, the magnetic structure of the compound can be seen as magnetic planes, formed by Co^{2+} in a state of high spin (HS) at sites 1, 2, and 3, separated by nonmagnetic planes, formed by Co^{3+} in LS states at sites 4. Above T_c, up to at least ~550 K a gradual Co^{3+} spin-state crossover (from LS to HS) seems to occur [10]. Lattice parameter anomalies between 400 and 500 K were also observed [10].

Doping the $Co_3O_2BO_3$ ludwigite with nonmagnetic ions generally enhances the magnetism and increases the T_c [2,4]. This feature is attributed mainly to three effects: the nonmagnetic ions place only at site 4 (low structural disorder), the absence of a double-exchange interaction (remove the competition between exchange interactions), and the appearance of Co^{2+} ions in a HS state at sites 4 (substituting the LS Co^{3+}) that couple the magnetic layers. On the other hand, when the $Co_3O_2BO_3$ ludwigite is doped with other metallic magnetic ions, the dopant ion occupies almost all the sites in the structure, giving rise to structural disorder [5,11]. This, together with the different valence and spin of the dopant, increases the competition between the exchange interactions giving rise to magnetic disorder, such that a spin-glass state is commonly established [5,11]. The structural disorder caused

*dalbersanchez@id.uff.br

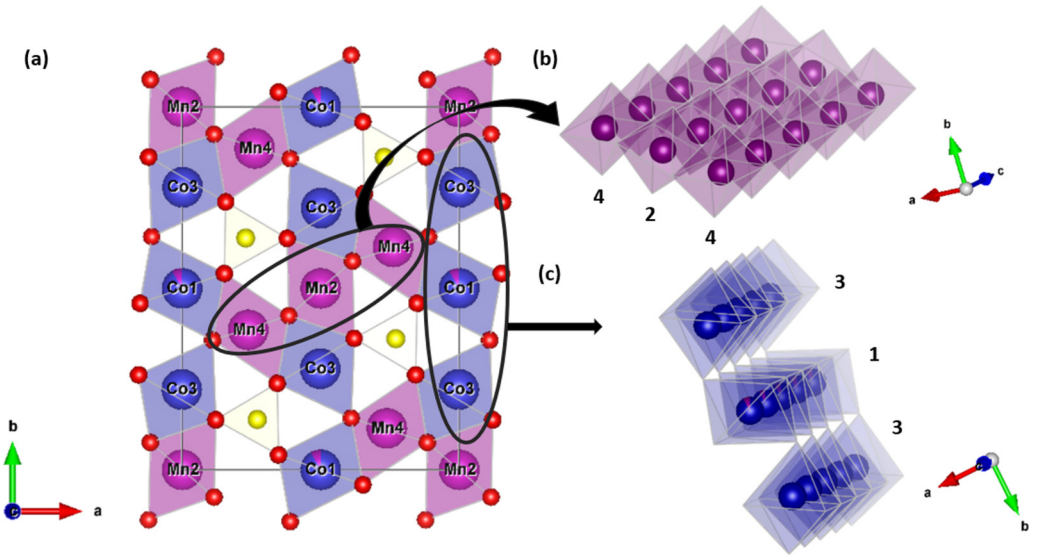

FIG. 1. (a) Crystalline structure of the ludwigite projected on the *ab* plane. The continuous line represents the unit cell, the yellow spheres represent the boron atoms and the red spheres represent the oxygen atoms. (b) The 4-2-4 substructure composed only of Mn ions shown in the perspective of the ladder. (c) The 3-1-3 substructure composed mainly of Co ions with a very small amount of Mn (2.6% of the Co ions) shown in the perspective of the ladder. These figures were generated by the VESTA software [6].

by the doping ions impedes a correct evaluation of the influence of each exchange interaction on the magnetic properties of these compounds.

The synthesis of structurally ordered heterometallic ludwigites with two magnetic cations has been until now unsuccessful. Such systems involve all types of exchange interactions and should allow in principle to study the effect of each of these interactions separately. Actually, the unique structurally ordered ludwigite that contains two metallic cations is $Ni_5Sn(O_2BO_3)_2$ [12]. In this compound the Ni and Sn ions are alternately located at sites 4 along the *c* axis. However, it has only one magnetic ion and a unique type of exchange interaction, the superexchange. In spite of the absence of competing exchange interactions this compound does not show full long-range magnetic order and just a partial magnetic ordering was observed at 73 K [12].

In this work we report the synthesis and characterization of the heterometallic $Co_3Mn_3(O_2BO_3)_2$ ludwigite. The x-ray results show an almost structurally ordered compound with Co ions occupying sites 1 and 3 and Mn sites 4 and 2. This implies that the three-legged ladders 3-1-3 are formed exclusively by Co ions (except for a very small amount of Mn at site 1), as in the $Co_3O_2BO_3$, and the 4-2-4 ladders contain only Mn ions. So, structurally this compound can be seen as consisting of two subsystems, each containing a unique magnetic ion. From the point of view of the magnetism, the partition in two magnetic subsystems formed by a unique magnetic ion could, in principle, inhibit the magnetic disorder. However, the experimental results presented here reveal an unexpected behavior. The compound does not exhibit long-range magnetic order and a spin-glass state is established at 31.9 K. The magnetic data analysis indicates that Co^{2+}, Mn^{2+}, and Mn^{3+} are present in HS states. This compound surprisingly shows the highest degree of magnetic disorder as indicated by specific heat measurements. Our results show that the competition between direct-, super-, and double-exchange interactions between the Mn^{2+} and Mn^{3+} give rise to strong magnetic frustration in the 4-2-4 ladder that, along a weak disorder, due to the presence of a very small amount of Mn at site 1, has a direct influence in the establishment of a long-range magnetic order throughout the compound.

II. EXPERIMENT

A. Sample preparation

The crystals were synthesized from a 12:12:8 molar mixture of $CoO:MnO_2:H_3BO_3$, respectively, and with 10 g of borax ($Na_2B_4O_7$). This mixture was heated at 1100 °C for 24 h and after that cooled down to 600 °C for 48 h. Then the oven was turned off. The final product was dissolved in hot water and the crystals cleaned in an ultrasonic bath at 50 °C. Needle-shaped black crystals up to 0.2 mm in length were obtained.

B. X-ray diffraction

Several needle-shaped crystals were used to collect x-ray diffraction data on single crystals. The measurement single-crystal x-ray diffraction was done using a D8 Venture Bruker diffractometer at 150 K, using Incoatec Microfocus Source (IμS) x ray, Mo $K\alpha$ radiation. The crystal was mounted on a Kappa goniometer, and the data were collected using a PHOTON 100 detector. Data collection was performed with APEX [13]. Multiscan correction using equivalent reflections was applied. The full-matrix least-squares refinements based on F^2 with anisotropic thermal parameters were carried out using SHELXL-2013 [14] program packages with WINGX [15] and SHELXLE [16] software interfaces.

Crystal data, data-collection parameters, and structure refinement data are displayed in Table I. The crystallographic tables were generated by WINGX [15]. We remark that the complete structure, except for the boron ions, may be obtained

TABLE I. Crystal data and structure refinement of the $Co_3Mn_3(O_2BO_3)_2$ at 150 K.

Empirical formula	$Co_{2.922}Mn_{3.078}B_2O_{10}$
Formula weight	523.23
Wavelength	0.717073 Å
Temperature	150(2) K
Crystal system	orthorhombic
Space group	*Pbam*
Unit cell dimension, a	9.2101(5) Å
b	12.0603(7) Å
c	3.0055(2) Å
Volume	33.84(3) Å^3
Z	2
Density (calculated)	5.205 Mg/m^3
Crystal size (μm^3)	200 × 50 × 40
Absorption coefficient	12.837/mm
F(000)	492
θ range	2.783° to 36.806°
Index range, h	−15, 15
k	−20, 20
l	−5, 5
Reflections collected	30 830
Independent reflections	960
R(int)	0.0533
Completeness to $\theta = 25.242$	100%
Refinement method	Full-matrix least-squares on F^2
Data/restraints/parameters	960/0/58
Goodness of fit on F^2	1.233
Final R indices [$I > 2\,\sigma$(I)]	$R1 = 0.0305$, $wR2 = 0.0807$
R indices (all data)	$R1 = 0.0370$, $wR2 = 0.0829$
Extinction coefficient	0.0047(11)
Largest diff. peak	1.284 e Å^{-3}
Largest diff. hole	−1.646 e Å^{-3}

from the two three-legged-ladder subunits formed, respectively, by the metal sites 4-2-4 and 3-1-3. Sites 1 are almost fully occupied by Co ions (92.2%) with a small amount of Mn (7.8%), which represent 1.3% of the total ions and sites 3 are occupied only by Co atoms. Sites 2 and 4 are exclusively occupied by Mn (see Fig. 1). From the x-ray analysis we arrived at the chemical composition for our compound, $Co_{2.922}Mn_{3.078}(O_2BO_3)_2$, in this paper denoted as $Co_3Mn_3(O_2BO_3)_2$. Table II shows the fractional coordinates and the site occupation factor. The intermetallic distances in this compound are shown in Table III. Table IV shows the bond lengths between Co or Mn and oxygen in an octahedral coordination.

Powder x-ray diffraction experiments were performed to check the presence of impurities in our sample. The room-temperature x-ray pattern of the $Co_3Mn_3(O_2BO_3)_2$ was compared with that simulated from the single-crystal refinement at the same temperature (see Fig. 2) and no extra peaks were observed, indicating a single-phase sample, ruling out the presence of any impurity phase. From the Co-O and Mn-O distances, we can estimate the oxidation numbers for the ions in each crystallographic site by using the bond valence sum (BVS) calculations [18]. We applied the formulas given by Liu and Thorp [18] to get the oxidation numbers Z_j of the Co

TABLE II. Atomic coordinates and site occupation factor (SOF) for $Co_3Mn_3(O_2BO_3)_2$ at 150 K. U(eq) (10^{-3} Å) is defined as one-third of the trace of the orthogonalized U_{ij} tensor.

Site	x/a	y/b	z/c	SOF	U(eq)
Co(1)	1/2	1/2	0	0.2305	3(1)
Mn(1)	1/2	1/2	0	0.0195	3(1)
Mn(2)	1/2	0	1/2	1/4	5(1)
Co(3)	0.4982(1)	0.2214(1)	0	1/2	2(1)
Mn(4)	0.2385(1)	0.1141(1)	1/2	1/2	5(1)
O(1)	0.6102(3)	0.3578(2)	0	1/2	8(1)
O(2)	0.3477(3)	0.4588(2)	1/2	1/2	6(1)
O(3)	0.3423(3)	0.2614(2)	1/2	1/2	5(1)
O(4)	0.3848(3)	0.0751(2)	0	1/2	15(1)
O(5)	0.6210(3)	0.1373(2)	1/2	1/2	4(1)
B	0.2704(4)	0.3609(3)	1/2	1/2	4(1)

and Mn ions at sites j:

$$Z_j = \sum_i s_{ij}, \tag{1}$$

where $s_{ij} = \exp[(R_0 - r_{ij}/b)]$, R_0 and b are parameters given in Ref. [18], and r_{ij} are the distances from the metal ion to the oxygen ions in the octahedron. Table V shows the valence state found for the metals ions at different sites in the structure.

From these results we can ascribe 2+ valence for all cobalt ions. With the parameter for Mn^{2+} the calculations give 2.921 and 3.101 for the valences of the Mn at sites 2 and 4, respectively. With the Mn^{3+} parameters the corresponding values become 2.671 and 2.837. According to charge balancing, the total charge on the 4-2-4 ladder should be 8+. Through the BVS calculations we find 8.345+, assuming Mn^{3+} in both sites. This may be indicative of an electron shared between sites 2 and 4.

With the structural parameters it is also possible to estimate the ion radii r_0 through the root of the harmonic mean square (rhms):

$$r_0 = \left[\frac{1}{6}\sum \frac{1}{(d_i - 1.40)^2}\right]^{-1/2}, \tag{2}$$

where 1.40 is an estimate of the oxygen radius (in Å) and d_i are the distances between the ion and the oxygens [19,20]. The

TABLE III. Selected bond lengths (in Å), between the metallic ions, for the ludwigite $Co_3Mn_3(O_2BO_3)_2$ at 150 K compared with the Co and Fe homometallic at room temperature. Here, i, j are the crystallographic positions. The subscript is the symmetry code (i) $-x + 3/2, y - 1/2, -z - 1$.

d_{j-k}	$Co_3O_2BO_3$ [8]	$Fe_3O_2BO_3$ [17]	$Co_3Mn_3(O_2BO_3)_2$
d_{j-j}	2.9627(1)	3.0780(10)	3.0055(3)
d_{4-3}	3.0868(5)	3.1881(5)	3.1071(7)
d_{2-3}	3.0539(4)	3.1755(6)	3.0637(5)
d_{4-2}	2.7510(4)	2.7849(4)	2.7739(6)
d_{4-1i}	3.0092(3)	3.1031(4)	2.9957(5)
d_{1-3}	3.3008(5)	3.3744(4)	3.3604(6)

TABLE IV. Selected bond lengths between Co or Mn and oxygen ions (in Å) for $Co_3Mn_3(O_2BO_3)_2$ at 150 K. The subscript is the symmetry code: (*i*) $x-1/2, -y+1/2, z$.

$Co(Mn)_1$–O_1	1.993(3)	Co_3–O_4	2.050(3)
$Co(Mn)_1$–O_2	2.1150(18)	Co_3–O_5	2.1369(18)
Mn_2–O_4	2.0509(19)	Mn_4–O_{1i}	1.9412(17)
Mn_2–O_5	1.997(3)	Mn_4–O_2	2.033(3)
Co_3–O_1	1.942(3)	Mn_4–O_3	2.018(3)
Co_3–O_3	2.1339(19)	Mn_4–O_4	2.0722(19)

values of d_i are shown in Table IV and the estimated rhms radii for the Mn at site 4 is 0.61 Å, which agrees with the value 0.59(1) estimated for the Mn^{3+} [19]. Analogously, the rhms radii found for the Mn at site 2 is 0.64, a value not as high as expected for Mn^{2+} but greater than that for site 4. These results indicate an oxidation state between 2+ and 3+ for the Mn ions.

Another important parameter related to the magnitude of the Jahn-Teller distortion is the edge length distortion (ELD), defined as [21,22]

$$\mathrm{ELD} = \frac{100}{n}\sum_{i}^{n}\frac{|OO_i - \langle OO\rangle|}{\langle OO\rangle} \tag{3}$$

where OO_i is the edge length of the polyhedron and $\langle OO\rangle$ is the average edge length.

The ELD values calculated for sites 2 and 4 of our compound are 3.82% and 5.01%, respectively.

C. Magnetic measurements

The magnetic measurements were performed on powdered samples of $Co_3Mn_3(O_2BO_3)_2$ using a commercial Physcial Properties Measurement System (PPMS) platform from Quantum Design. Figure 3 shows the temperature dependence of magnetization curves for zero-field-cooled (ZFC) and field-cooled (FC) processes, with applied magnetic field of 100 Oe. Lowering the temperature, an appreciable increase in magnetization below ∼5 K is observed. A shoulder appears in the ZFC magnetization curve at ∼50 K and below this temperature the magnetization increases drastically, reaching a maximum value at ∼31 K.

TABLE V. Oxidation numbers for the Co and Mn ions in $Co_3Mn_3(O_2BO_3)_2$ obtained by using the bond valence sum (BVS) [18].

Co_1	2.094
Mn_2	2.671
Co_3	2.029
Mn_4	2.837

The inset shows that the temperature dependence of the inverse of the susceptibility is linear above 150 K and can be well described by the Curie-Weiss law. From the Curie-Weiss law fitting (see inset of Fig. 3) we get a Curie constant $C = 20.00 \times 10^{-3}$ emu K/(g Oe) and a small Curie-Weiss temperature $\theta_{CW} = -8.84$ K, indicating similar strengths for the ferromagnetic and antiferromagnetic interactions. Using the Curie constant we determine the effective moment per formula unit, $\mu_{\mathrm{eff}} = 12.95\mu_B$. The calculation of the mean effective momentum per unit formula considering only the spin momentum ($g = 2$) for Co^{2+} ($S = 3/2$), Mn^{3+} ($S = 2$), and Mn^{2+} ($S = 5/2$) gives $\mu_S = \sqrt{\sum_i n_i g_i^2 S_i(S_i+1)} = 11.31\mu_B$ (where n_i is the number of i ions per unit formula), a value somewhat smaller than that found experimentally. Thus the experimental results indicate an orbital contribution to the total magnetic moment of the Co^{2+}, as observed previously in other Co ludwigites [2,4,8].

Figure 4 shows the real and imaginary parts of the ac susceptibility (χ') as a function of temperature and for different frequencies. There we can observe a rather

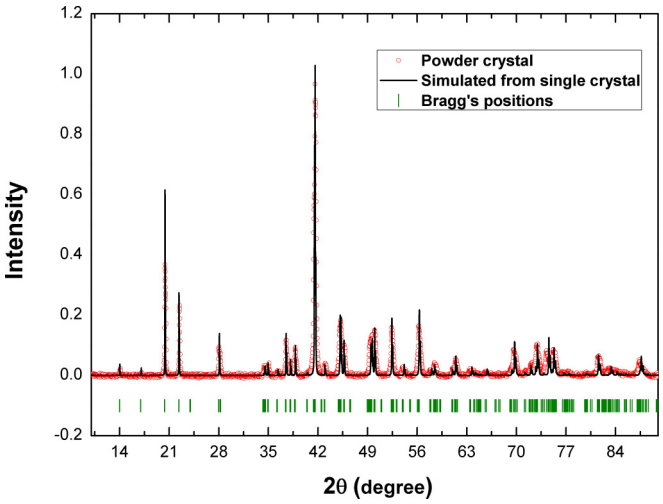

FIG. 2. Room-temperature powder x-ray diffraction pattern (red circles) and the simulated one obtained from the analysis of the single-crystal x-ray data at the same temperature (solid line) for $Co_3Mn_3(O_2BO_3)_2$. The allowed Bragg positions are shown as vertical green bars.

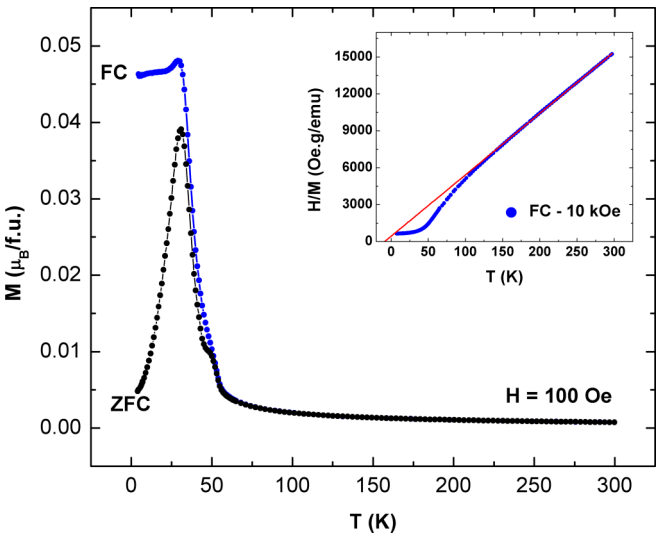

FIG. 3. Magnetization versus temperature for $Co_3Mn_3(O_2BO_3)_2$ ludwigite under an applied magnetic field of 100 Oe. Inset: Inverse magnetization in a 10-kOe magnetic field.

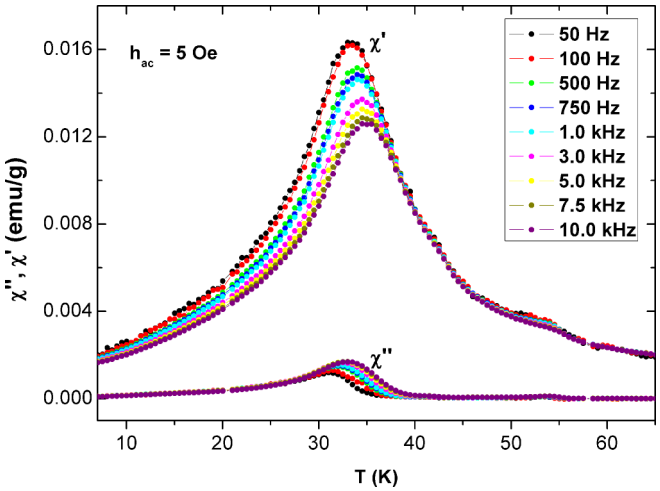

FIG. 4. Real (χ') and imaginary (χ'') parts of $Co_3Mn_3(O_2BO_3)_2$ ac magnetic susceptibility as functions of temperature for frequencies from 0.05 to 10 kHz. The amplitude of the oscillating magnetic field is 5 Oe.

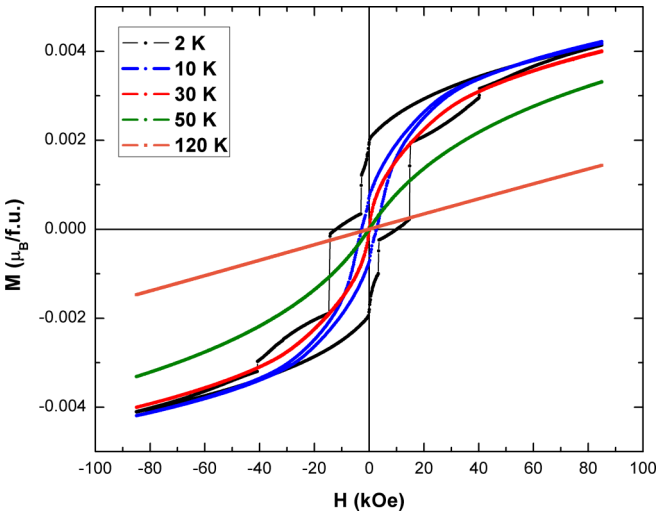

FIG. 6. Hysteresis loops for the powdered $Co_3Mn_3(O_2BO_3)_2$ compound at 2, 10, 30, 50, and 120 K.

broadened peak centered at ∼31 K, the same temperature at which a spontaneous magnetization was observed in the ZFC and FC magnetization curves. A small kink is clearly observed at ∼50 K in the real and imaginary ac susceptibility curve (see Fig. 4). The position of the peak changes with frequency, indicating a possible spin-glass state. A signature of the spin-glass systems is that they follow the critical dynamics scaling law [Eq. (4)]; that is, the relaxation time τ diverges at T_g as

$$\tau = \tau_0 \left(\frac{T}{T_g} - 1 \right)^{-z\nu}, \tag{4}$$

where τ_0 represents the microscopic flipping time of the fluctuating spins, T_f the frequency-dependent freezing temperature, T_g the spin-glass phase-transition temperature, and $z\nu$ the critical exponent. A detailed analysis of the frequency dependence of $\chi'(T)$ using the critical dynamics scaling law

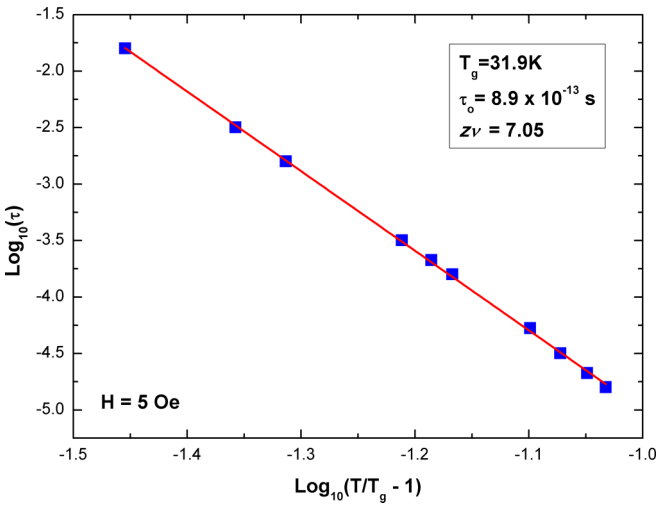

FIG. 5. The best fit of relaxation times using to the power law for ac susceptibility with applied field of 5 Oe for $Co_3Mn_3(O_2BO_3)_2$.

provides unequivocal evidence for the appearance of spin glass in $Co_3Mn_3(O_2BO_3)_2$ below $T_g = 31.9$ K (see Fig. 5).

The frequency shift of T_f is given by the empirical parameter $X = (\Delta T_f/T_f)(\Delta(\log \omega)$ [23]. For $Co_3Mn_3(O_2BO_3)_2$ we get $X = 0.02$, also χ'' is 10% of χ', typical values for insulating spin glasses.

Figure 6 shows hysteresis curves for different temperatures. Above 50 K the linear and closed hysteresis loop are typical of a paramagnetic state. The closed hysteresis loop at 50 K suggests an antiferromagnetic state, in agreement with the specific heat results as will be discussed later. Below 31 K the hysteresis loops become open with both the coercive field and the remanent magnetization increasing as the temperature decreases. A maximum coercive field of ∼11 kOe and remanent magnetization $\sim 0.002\mu_B$ per formula unit is achieved at 2 K. At 2 K the hysteresis loop present jumps, a feature compatible with ferro- or ferrimagnetic arrangements of the spins or with a spin-glass phase [5]. Even at an external magnetic field of 9 T it was not possible to reach magnetic saturation, indicating strong anisotropic effects.

D. Specific heat measurements

Specific heat measurements as a function of temperature were performed in a polycrystalline sample under external applied magnetic field (Fig. 7). No sharp feature is observed in the specific-heat curve of $Co_3Mn_3(O_2BO_3)_2$, apparently ruling out any phase transition up to at least 200 K, the highest temperature of the measurements. The specific heat presents a broad maximum well above the freezing temperature as usual in spin glasses.

The low-temperature ($T < 7$ K) specific heat data were best analyzed using the power law $C = \gamma T + \alpha T^2$ as shown in Fig. 8. The parameters calculated from these analyses are presented in Table VI. Notice the presence of a large linear term associated with the spin-glass state in this insulating material. Also we point out that the phonon contribution is expected to be very small at these temperatures.

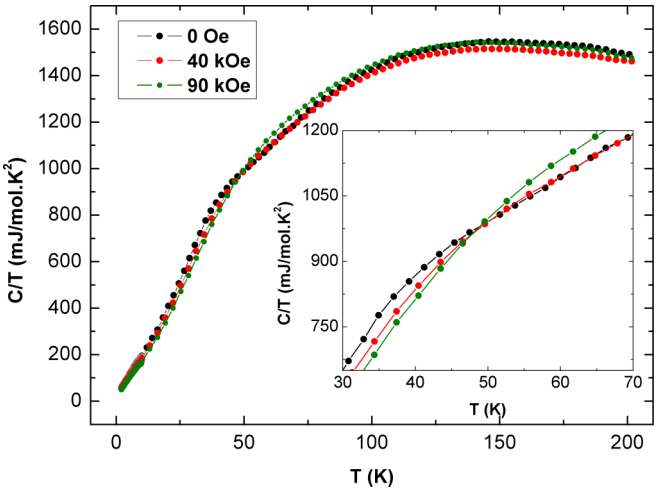

FIG. 7. Specific heat of $Co_3Mn_3(O_2BO_3)_2$ represented as C/T versus T for 0 Oe, 40 kOe, and 90 kOe fields. Inset: Zoom of the region where the intersection of the curves for the different fields occurs.

A T^2 contribution to the specific heat arises from excitations with a linear dispersion relation, like phonons, antiferromagnetic magnons, or both in a two-dimensional structure [4,24].

III. DISCUSSION

Using the flux method we synthesized the $Co_3Mn_3(O_2BO_3)_2$ system, with a unique structure among the ludwigites. Several crystals were analyzed by single-crystal x-ray diffraction and the experiments have shown that half of the metallic ions are Co and half Mn, implying the empirical formula $Co_{2.92}Mn_{3.08}(O_2BO_3)_2$. This compound is completely different from the reported $Co_{1.7}Mn_{1.3}O_2BO_3$,

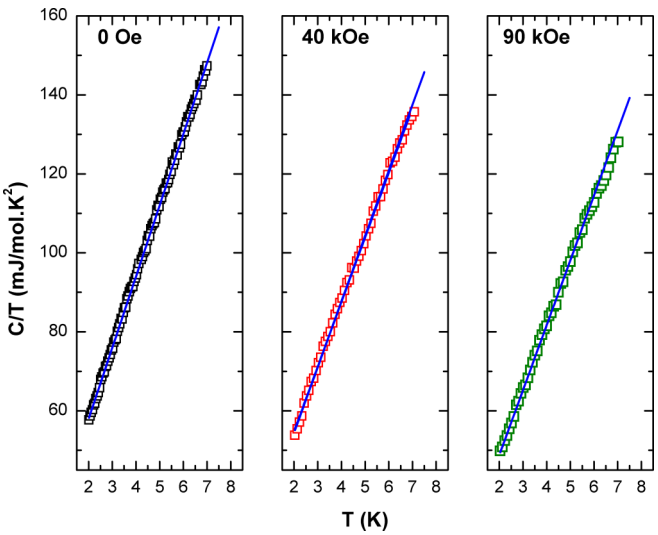

FIG. 8. Specific heat of $Co_3Mn_3(O_2BO_3)_2$ represented as C/T versus T for 0 Oe, 40 kOe, and 90 kOe fields. The parameters of the linear fittings are shown in Table VI.

where the Mn^{2+} and Mn^{3+} occupy all the metallic available sites [11] and from $Co_{2.5}Mn_{0.5}O_2BO_3$ where the Mn^{4+} occupy site 4 exclusively [25]. The most interesting feature of $Co_3Mn_3(O_2BO_3)_2$ is that in this material the ions are grouped in a particular way never seen before in ludwigites. They form two subsystems, each containing a single type of ion: the 4-2-4 ladder is composed exclusively of Mn ions and the 3-1-3 ladder contains only Co ions, except for a small amount of Mn at sites 1. As discussed below, this particular arrangement seems to have drastic consequences for the establishment or not of long-range magnetic ordering.

Through BVS calculations, it was possible to ascribe a valence state of 2+ for all Co ions in the 3-1-3 ladder. On the other hand, it was not possible to attribute an integer valence state for the Mn ions and values of 2.671 and 2.837 were obtained for the Mn at sites 2 and 4, respectively. For a correct charge balance, the Mn ions at sites 2 and 4 should have, on average, a valence state of 2.7, meaning that in the 4-2-4 ladder two of these sites should have a valence state of 3+ and one a valence 2+. Besides, the 4-2-4 ladder can be described as three Mn^{3+} sharing an extra electron. According to the values found for the valence, the extra electron in the 4-2-4 ladder may be considered to be located mainly in the columns of sites 2. This feature is not uncommon in ludwigites; in $Fe_3O_2BO_3$, for example, the Fe ions at sites 2 and 4 are sharing an electron [7]. These results indicate that a charge ordering phenomenon, in which the extra electron localizes in one of these sites, may occur in $Co_3Mn_3(O_2BO_3)_2$ and should be further investigated.

The analysis of the inverse magnetization of the paramagnetic region using the Curie-Weiss law gives a small negative θ_{CW} indicating a slight predominance of the antiferromagnetic interactions. The value of the effective magnetic moment is compatible with a quenched orbital moment of the Mn^{3+} ions at site 4, but not for Co^{2+}.

The warwickite Mn_2BO_4, with two nonequivalent sites for the metal, occupied by Mn^{2+} and Mn^{3+} which are octahedrally coordinated, has an orbital ordering of the Jahn-Teller Mn^{3+} states [20,26]. A measure of the magnitude of the Jahn-Teller distortion is given by the octahedral distortion parameter EDL [21,23]. For the orbitally ordered Mn^{3+} at site 1 of the Mn_2BO_4 the value is 6.8%, for the Mn^{3+} at site 4 of $Co_3Mn_3(O_2BO_3)_2$ the value is 5.01%, a value not so high as that of the former compound but larger than that of the also orbitally ordered Mn^{3+} in the henritermierite $Ca_3Mn_2[SiO_4]_2[O_4H_4]$ whose value is 3.4% [22]. So, the distortion degree of the Mn^{3+} at site 4 indicates a possible orbital ordering state for this ion. While Mn^{3+} is a strong Jahn-Teller ion, Mn^{2+} is an S state with small coupling to the lattice. A possible charge ordering configuration in our system is that the extra electron in the 4-2-4 ladder is localized at site 2, giving rise to Mn^{2+} with a small EDL. This is different from the transverse charge density wave transition occurring in the Fe homometallic ludwigite where the localization occurs in alternating sites 4, implying the doubling of the c-axis lattice parameter [17].

As pointed out before, a moderate increase of the magnetization occurs at ~50 K, the same temperature at which a tiny kink is observed in the real and imaginary parts of the

TABLE VI. Parameters γ, α, and β obtained from the fitting of the low-temperature specific heat data (Fig. 8) of the ludwigite $Co_3Mn_3(O_2BO_3)_2$. PW, present work.

	H (kOe)	γ [mJ/(mol K^2)]	α [mJ/(mol K^3)]	β [mJ/(mol K^4)]	Ref.
$Co_3Mn_3(O_2BO_3)_2$	0	21.90 ± 0.20	18.03 ± 0.04		PW
$Co_3Mn_3(O_2BO_3)_2$	40	21.20 ± 0.62	16.61 ± 0.17		PW
$Co_3Mn_3(O_2BO_3)_2$	90	15.85 ± 0.32	16.45 ± 0.08		PW
$Co_3O_2BO_3$	0	3.30		0.72	[8]
$Co_3O_2BO_3$	90	3.48		0.70	[8]
$Co_5Ti(B_2O_3)_2$	0	15.5		3.94	[5]
$Co_5Ti(B_2O_3)_2$	30	6.88		2.78	[5]
$Co_5Ti(B_2O_3)_2$	90	3.61		2.76	[5]
$Co_5Sn(B_2O_3)_2$	0	0.54		0.65	[2]
$Co_5Sn(B_2O_3)_2$	90	0.00		0.66	[2]

ac susceptibility curves (see Fig. 4). On the other hand, the specific heat measurements as a function of temperature in Fig. 7 show a crossing of the curves in zero and in external magnetic fields at approximately this same temperature. The existence of an additional contribution for $T \lesssim 50$ K in large fields is reminiscent of a metamagnetic transition where long-range antiferromagnetic order is destroyed by the magnetic field. These features suggest that $Co_3Mn_3(O_2BO_3)_2$ is close to an antiferromagnetic ordering at ∼50 K, but this long-range order is aborted by the strong frustration due to several competing interactions.

The magnetization increases with decreasing temperature, reaching a maximum value at ∼31 K and decreases for lower temperatures (Fig. 3). The ac susceptibility curve also shows a rather wide peak centered at the same temperature (Fig. 4). The frequency dependence of the χ' maximum temperature shows a clear spin-glass signature, a feature that was checked by the analysis of temperature dependence of the relaxation time with the critical scaling formula, giving a critical exponent $z\nu = 7.05$ and an effective spin-flip time $\tau_0 = 8.9 \times 10^{-13}$ s, typical of atomistic, dilute spin-glass systems [27–32]. The spin-glass transition temperature is $T_g = 31.9$ K. The spin-glass nature of the magnetic transition of our compound is corroborated through the analysis of low-temperature specific heat measurements. The coefficient of the linear temperature-dependent contribution to the specific heat, $\gamma = 21.9$ mJ/(mol K^2) at zero field, is the largest found for the ludwigites (see Table VI). This large value shows a strong competition between the magnetic interactions and consequently a high degree of frustration, compatible with a spin-glass system.

It is not a surprise that a spin-glass state occurs in ludwigites as already reported in $CoMgGaO_2BO_3$, $Co_2AlO_2BO_3$, and $Co_5Ti(O_2BO_3)_2$. The diamagnetic dilution of the $Co_3O_2BO_3$ with nonmagnetic Mg, Ga, Al, and Ti ions weakens the magnetic interactions. Besides, these nonmagnetic ions occupy all the available metallic sites producing a positional disorder leading to the establishment of a spin-glass state. If we take into account that, in $Co_5Sn(O_2BO_3)_2$ with the Sn ion placed only at site 4, the magnetic interactions are strengthened and long-range magnetic order takes place [2], the *positional disorder* seems to be the key factor that leads to a spin-glass ground state in these kinds of compounds [5,26,33].

The effects caused by doping with magnetic ions are similar to those produced by nonmagnetic ions. For example, in $Co_2FeO_2BO_3$, the Fe ions occupy mainly sites 2 and 4 of the 4-2-4 ladders producing low positional disorder. Magnetic order, albeit partial, takes place at 117 K in this material [3,34]. The magnetic transition is related to the ordering of the Fe^{3+} in the 3LL, reminiscent of the magnetic transition in the $Fe_3O_2BO_3$. The remaining magnetic ions seem to freeze below 70 K and a complex magnetic structure for the Fe-Co system is established at low temperature [8]. On the other hand, in $Co_{1.7}Mn_{1.3}O_2BO_3$, synthesized by the solution method [11], the Mn^{2+} and Mn^{3+} magnetic ions spread throughout the compound and occupy four nonequivalent sites. The random distribution of the Mn ions in the compounds yield a high degree of positional disorder and consequently a spin-glass freezing of the magnetic ions at 41 K [11].

On the other hand, what is striking is that in a positionally ordered compound such as $Co_3Mn_3(O_2BO_3)_2$, a spin-glass phenomenon occurs. Magnetization measurements indicate that both Mn^{2+} and Mn^{3+} in sites 2 and 4 are in HS states and that the latter has a contribution of magnetic angular momentum. In order to understand the occurrence of a spin-glass state, we have to pay attention to what is happening in the low-dimensional 4-2-4 ladders. There, the smallest interatomic distances are found and the strongest magnetic interactions are expected to take place. As shown by x-ray experiments the 4-2-4 ladder is a planar substructure consisting of edge-sharing MnO_6 octahedra (see Fig. 1).

For this particular arrangement all the magnetic interactions between the Mn^{2+} ($t_{2g}^3 e_g^2$) and Mn^{3+} ($t_{2g}^3 e_g^1$) are present, i.e., the superexchange (for 90° and 180° Mn-O-Mn angles), double-exchange, and direct-exchange interactions. Depending on the hierarchical order of these interactions, a magnetic ordering may be established, as happens in many ludwigites [2,3,9], or it may lead to a state of strong magnetic frustration (spin glass) [5,26,33].

In the $MnTiO_3$ ilmenite the MnO_6 octahedra are edge sharing and form magnetic planes which are separated by nonmagnetic Ti^{4+} ions. Long-range magnetic ordering sets in at 63.6 K. Inside the planes the arrangement of the spins is antiferromagnetic and the magnetic planes are stacked along the c axis [21,26]. For this compound with only Mn^{2+} the double-exchange interaction is ruled out. Taking into account that all Mn-O-Mn bonds in the magnetic planes are close to

90° (88.4°), it is possible to assume that the 88.4° superexchange is the dominant interaction. In this case the direct interaction between the t_{2g} orbitals of the Mn ions is expected to be small due to the separation between the ions, which in this case is $d = 3.067$ Å. The magnetic planes are 3.998 Å apart and the magnetic interaction between them occurs through the Mn-O-O-Mn bonds [35].

The $Mn_2B_2O_5$ pyroborate has ribbon-shaped substructures formed by octahedrally coordinated Mn^{2+} ions [36]. For coplanar ribbons, the shortest distances between Mn ions are 4.522 and 4.446 Å. For ribbons in adjacent planes, the shortest distances between Mn ions are 4.198 and 4.113 Å. Within the ribbon, the Mn-O-Mn bonds angles are between 95.28° and 103.60°, and Mn-Mn interatomic distances are between 3.179 and 3.274 Å [28,29]. Here the double-exchange interactions are ruled out too and all superexchange interactions involve bonding angles close to 90°. Due to the large interatomic distances between Mn ions, the direct-exchange interactions are expected to be small. Therefore, as in the case of the $MnTiO_3$ ilmenite, the superexchange interactions with 90° Mn-O-Mn bonds seem to determine the spin ordering and magnetic properties of this compound.

The most representative compound with edge-sharing MnO_6 octahedrons is the MnO, where all the Mn have a valence state of 2+ [37]. MnO is antiferromagnetically ordered at 119 K and exhibits a magnetic arrangement of spins in accordance with the Goodenough-Kanamori rules [37]. The distances between Mn ions with 90° Mn-O-Mn bonding angle is $d = 3.144$ Å, while that for the 180° bonding angle is $d = 4.460$ Å. As in the previous compounds, here the double-exchange interaction is excluded and the direct-exchange interaction between the t_{2g} orbitals is expected to be weak too. The superexchange interactions with 180° and 90° bonds become dominant and the competition between them determines the magnetic properties of this compound.

Among other compounds with structure similar to the 4-2-4 ladders that show competition between double- and superexchange interactions is the Mn_2OBO_3 warwickite. The Mn ions are found inside oxygen octahedra that share their edges and form four-line-wide ribbon-shaped substructures [20]. These lines are parallel to the c axis and contain two different crystallographic sites. Divalent ions Mn^{2+} occupy lateral line positions and trivalent ions Mn^{3+} occupy centerline positions. This charge ordering persists up to high temperatures [38]. The axially elongated Mn^{3+} octahedra revealed an orbital order [39,40]. Within the ribbons the octahedrons share their edges and the Mn-O-Mn bonding angles lie between 88.6° and 105.3°. The separation between the Mn ions is, on average, 3.324 Å. This separation between Mn ions indicates a small direct interaction. Thus, oxygen-mediated superexchange and double-exchange interactions with Mn-O-Mn angles of ∼100° become dominant. This compound presents a long-range antiferromagnetic transition below 26 K [26]. The Mn-O-Mn superexchange interactions on the ribbon adopt a ferromagnetic or antiferromagnetic character according to the orbital ordering of the Mn^{3+}, that is, to the electronic density e_g at the Mn-O bonds. Neutron measurements are consistent with most of the superexchange interactions predicted by the Goodenough-Kanamori rules. It should be noted here that all exchange interactions involve only Mn-O-Mn bonds close to 90°. There are not exchange interactions involving 180° bonds.

As discussed above for the previous ordered compounds, they present long-range magnetic order. Superexchange interactions are dominant and are responsible for the type of magnetic order and hence for their magnetic properties. Within this picture one might expect that the three-legged ladder 4-2-4, the subsystem formed exclusively of octahedrally coordinated Mn ions in $Co_3Mn_3(O_2BO_3)_2$, should lead to a magnetic ordering. However, this does not happen and only a spin-glass state is established. The three-legged ladder 4-2-4 of our compound differs from the systems mentioned above in that, besides superexchange and double-exchange interactions with 90° and 180° Mn-O-Mn bonding angles, we have the direct-exchange interaction. While in the other compounds it was possible to distinguish the dominant interactions, in our compound it is more difficult since we have all the possible interactions and now the direct interaction is stronger. In the compounds mentioned above, the distances between the ions are greater than 3.064 Å, which is the limit of the direct overlap of the d orbitals and the direct-exchange interaction is not relevant [41].

In the 4-2-4 ladder of our compound, the distance between the Mn ions is 2.7739 Å, which gives rise to a strong overlap of the d-d orbitals and, consequently, a strong direct-exchange interaction. Then in this compound the direct-exchange interactions compete equally with the other interactions, leading to a state of strong magnetic frustration. On the other hand, a similar situation occurs in the 4-2-4 ladder of the $Fe_3O_2BO_3$ ludwigite, where all exchange interactions are also present, and the distance between Fe^{2+} and Fe^{3+} ions is 2.787 Å. This is almost the same distance found for the separation of the Mn ions in our compound, but in $Fe_3O_2BO_3$ the ladder is magnetically ordered at 112 K. So, why do the 4-2-4 ladders of $Fe_3O_2BO_3$ order magnetically and the 4-2-4 ladder of $Co_3Mn_3(O_2BO_3)_2$ does not? The answer may lie in the difference of the ionic radii of the ions involved in each compound. Although the ionic radii of Fe^{3+} and Mn^{3+} are similar (0.645 Å), the ionic radius of Mn^{2+} (0.830 Å) is larger than that of Fe^{2+} (0.780 Å) [42]. This implies that the overlap of the $d\,t_{2g}$ orbitals is greater for Mn than for Fe and therefore direct-exchange interaction is more important in the 4-2-4 ladder of $Co_3Mn_3(O_2BO_3)_2$ than in the 4-2-4 ladder of $Fe_3O_2BO_3$. Therefore, direct-exchange interaction seems to play a predominant role in establishing a state of frustration in our compound. Positionally ordered frustrated systems exhibiting a spin-glass behavior are few and associated to some type of disorder. For example, the spin-glass behavior in $Y_2Mo_2O_7$ is attributed to a subtle disorder in the Mo-Mo distances [43,44], in $ZnCr_2O_4$ to a disorder caused by randomly replacing 3% of the Zn ions by Cd [45], and in $DyMnO_3$ to a randomness caused by magnetoelastic strains [46]. Thus the establishment of a spin-glass state in our frustrated sample could be related to the weak disorder due to a random occupation of a small fraction of Mn at site 1, almost fully occupied by Co ions, similar to what happens with $ZnCr_2O_4$ when 3% of the Zn ions are substituted by Cd ions [45].

IV. CONCLUSIONS

Single-crystal x-ray diffraction has shown that $Co_3Mn_3(O_2BO_3)_2$ is composed of two subunits each containing a unique type of ion. BVS calculations show that all sites in 3-1-3 ladders are occupied by Co^{2+} and that in the 4-2-4 ladder the Mn ions have no valence integer values and can be described as three Mn^{3+} sharing an extra electron which is more localized at site 2. Magnetization measurements indicate that orbital moments of the Mn^{3+} ions at sites 4 are quenched but not those of the Co^{2+}. The magnetization and specific heat suggest that $Co_3Mn_3(O_2BO_3)_2$ is close to an antiferromagnetic ordering at $T \sim 50$ K, but this long-range order is disrupted by the strong frustration due to several competing interactions between Mn ions. The arrangement and distances between Mn ions in the 4-2-4 ladder, hardly found in nature, makes possible the competition between all superexchange, double-exchange, and direct-exchange interactions. Among these, the direct interaction between the Mn ions in the 4-2-4 ladder is strongest and can compete equally with the other interactions, leading to an undefined hierarchical order of them. In fact, the dynamic scaling analysis of ac susceptibility data has shown that the compound experiences a spin-glass transition at $T_g = 31.9$ K. The analysis of the low-temperature specific heat puts in evidence a linear temperature dependence with a coefficient $\gamma = 21.9$ mJ/(mol K^2), which is the largest found in ludwigites. This indicates a high degree of frustration, consistent with the spin-glass state observed at low temperatures.

ACKNOWLEDGMENTS

Support from LDRX-UFF and the Brazilian agencies CAPES, CNPq, and FAPERJ is gratefully acknowledged.

[1] P. Bordet and E. Suard, Phys. Rev. B **79**, 144408 (2009).
[2] C. P. Contreras Medrano, D. C. Freitas, D. R. Sanchez, C. B. Pinheiro, G. G. Eslava, L. Ghivelder, and M. A. Continentino, Phys. Rev. B **91**, 054402 (2015).
[3] D. C. Freitas, M. A. Continentino, R. B. Guimarães, J. C. Fernandes, E. P. Oliveira, R. E. Santelli, J. Ellena, G. G. Eslava, and L. Ghivelder, Phys. Rev. B **79**, 134437 (2009).
[4] C. P. C. Medrano, D. C. Freitas, E. C. Passamani, C. B. Pinheiro, E. Baggio-Saitovitch, M. A. Continentino, and D. R. Sanchez, Phys. Rev. B **95**, 214419 (2017).
[5] D. C. Freitas, R. B. Guimarães, D. R. Sanchez, J. C. Fernandes, M. A. Continentino, J. Ellena, A. Kitada, H. Kageyama, A. Matsuo, K. Kindo *et al.*, Phys. Rev. B **81**, 024432 (2010).
[6] K. Momma and F. Izumi, J. Appl. Crystallogr. **44**, 1272 (2011).
[7] J. Larrea, D. R. Sánchez, F. J. Litterst, E. M. Baggio-Saitovitch, J. C. Fernandes, R. B. Guimarães, and M. A. Continentino, Phys. Rev. B **70**, 174452 (2004).
[8] D. C. Freitas, M. A. Continentino, R. B. Guimarães, J. C. Fernandes, J. Ellena, and L. Ghivelder, Phys. Rev. B **77**, 184422 (2008).
[9] D. C. Freitas, C. P. C. Medrano, D. R. Sanchez, M. N. Regueiro, J. A. Rodríguez-Velamazán, and M. A. Continentino, Phys. Rev. B **94**, 174409 (2016).
[10] C. W. Galdino, D. C. Freitas, C. P. C. Medrano, R. Tartaglia, D. Rigitano, J. F. Oliveira, A. A. Mendonça, L. Ghivelder, M. A. Continentino, D. R. Sanchez, and E. Granado, Phys. Rev. B **100**, 165138 (2019).
[11] Y. Knyazev, N. Ivanova, N. Kazak, M. Platunov, L. Bezmaternykh, D. Velikanov, D. Vasiliev, S. Ovchinnikov, and G. Yurkin, J. Magn. Magn. Mater. **324**, 923 (2012).
[12] S. Sofronova, L. Bezmaternykh, E. Eremin, A. Chernyshov, and A. Bovina, Phys. Status Solidi B **255**, 1800281 (2018).
[13] A. Saint, APEX3, version 17.3-0, Bruker Analytical X-ray Systems Inc., Madison, Wisconsin, USA (2017).
[14] G. M. Sheldrick, Acta Crystallogr. Sect. C **71**, 3 (2015).
[15] L. J. Farrugia, J. Appl. Crystallogr. **32**, 837 (1999).
[16] C. B. Hübschle, G. M. Sheldrick, and B. Dittrich, J. Appl. Crystallogr. **44**, 1281 (2011).
[17] M. Mir, J. Janczak, and Y. P. Mascarenhas, J. Appl. Crystallogr. **39**, 42 (2006).
[18] W. Liu and H. H. Thorp, Inorg. Chem. **32**, 4102 (1993).
[19] R. Norrestam, Z. Kristallogr. **209**, 99 (1994).
[20] R. Norrestam, M. Kritikos, and A. Sjödin, J. Solid State Chem. **114**, 311 (1995).
[21] E. Akhmatskaya, R. Nobes, V. Milman, and B. Winkler, Z. Kristallogr. **214**, 808 (1999).
[22] A. Friedrich, B. Winkler, W. Morgenroth, A. Perlov, and V. Milman, Phys. Rev. B **92**, 014117 (2015).
[23] J. Mydosh, *Spin Glasses: An Experimental Introduction* (CRC Press, Boca Raton, FL, 1993).
[24] D. C. Freitas, R. B. Guimarães, J. C. Fernandes, M. A. Continentino, C. B. Pinheiro, J. A. L. C. Resende, G. G. Eslava, and L. Ghivelder, Phys. Rev. B **81**, 174403 (2010).
[25] A. Utzolino and K. Bluhm, Z. Naturforsch. B **51**, 305 (1996).
[26] R. J. Goff, A. J. Williams, and J. P. Attfield, Phys. Rev. B **70**, 014426 (2004).
[27] M. Continentino and A. P. Malozemoff, Phys. Rev. B **34**, 471 (1986).
[28] R. Mathieu, D. Akahoshi, A. Asamitsu, Y. Tomioka, and Y. Tokura, Phys. Rev. Lett. **93**, 227202 (2004).
[29] R. Mathieu, A. Asamitsu, Y. Kaneko, J. P. He, and Y. Tokura, Phys. Rev. B **72**, 014436 (2005).
[30] S. Nair and A. K. Nigam, Phys. Rev. B **75**, 214415 (2007).
[31] D. N. H. Nam, R. Mathieu, P. Nordblad, N. V. Khiem, and N. X. Phuc, Phys. Rev. B **62**, 8989 (2000).
[32] P. Svedlindh, P. Granberg, P. Nordblad, L. Lundgren, and H. S. Chen, Phys. Rev. B **35**, 268 (1987).
[33] N. B. Ivanova, M. S. Platunov, Y. V. Knyazev, N. V. Kazak, L. N. Bezmaternykh, E. V. Eremin, and A. D. Vasiliev, Low Temp. Phys. **38**, 172 (2012).
[34] M. Platunov, S. Ovchinnikov, N. Kazak, N. Ivanova, V. Zabluda, E. Weschke, E. Schierle, and K. Lamonova, JETP Lett. **96**, 650 (2013).
[35] G. Shirane, S. J. Pickart, and Y. Ishikawa, J. Phys. Soc. Jpn. **14**, 1352 (1959).
[36] J. C. Fernandes, F. S. Sarrat, R. B. Guimarães, R. S. Freitas, M. A. Continentino, A. C. Doriguetto, Y. P. Mascarenhas, J. Ellena, E. E. Castellano, J.-L. Tholence *et al.*, Phys. Rev. B **67**, 104413 (2003).

[37] C. G. Shull, W. A. Strauser, and E. O. Wollan, Phys. Rev. **83**, 333 (1951).
[38] V. Gnezdilov, Y. Pashkevich, V. Kurnosov, O. V. Zhuravlev, D. Wulferding, P. Lemmens, N. V. Kazak, Y. V. Knyazev, and S. G. Ovchinnikov, Low Temp. Phys. **45**, 1046 (2019).
[39] C. P. C. Medrano, D. C. Freitas, E. C. Passamani, J. A. L. C. Resende, M. Alzamora, E. Granado, C. W. Galdino, E. Baggio-Saitovitch, M. A. Continentino, and D. R. Sanchez, Phys. Rev. B **98**, 054435 (2018).
[40] N. Kazak, M. Platunov, Y. Knyazev, N. Ivanova, O. Bayukov, A. Vasiliev, L. Bezmaternykh, V. Nizhankovskii, S. Gavrilkin, K. Lamonova *et al.*, J. Magn. Magn. Mater. **393**, 316 (2015).
[41] D. R. Hartree, J. Opt. Soc. Am. **46**, 350 (1956).
[42] R. D. Shannon, Acta Crystallogr. Sect. A **32**, 751 (1976).
[43] A. Keren and J. S. Gardner, Phys. Rev. Lett. **87**, 177201 (2001).
[44] C. H. Booth, J. S. Gardner, G. H. Kwei, R. H. Heffner, F. Bridges, and M. A. Subramanian, Phys. Rev. B **62**, R755 (2000).
[45] W. Ratcliff, II, S.-H. Lee, C. Broholm, S.-W. Cheong, and Q. Huang, Phys. Rev. B **65**, 220406(R) (2002).
[46] P. A. Kumar, A. Kumar, K. Kumar, G. A. Babu, P. Vijayakumar, S. Ganesamoorthy, P. Ramasamy, and D. Pandey, J. Phys. Chem. C **123**, 30499 (2019).